Dalton Transactions

ROYAL SOCIETY OF CHEMISTRY

PAPER

View Article Online
View Journal | View Issue

Cite this: *Dalton Trans.*, 2025, **54**, 1980

Electronic structures of blue copper centers of amicyanin and azurin in the solution state†

Yudai Izumi, ‡§[a] Ralph Ugalino,§[a,b] Jun Miyawaki,[b] Chie Shibazaki,[c] Motoyasu Adachi,[a] Naoya Kurahashi,¶[d] Hisao Kiuchi,[d] Yoshihisa Harada[d] and Kentaro Fujii *[a,b]

Received 15th October 2024,
Accepted 4th December 2024

DOI: 10.1039/d4dt02891k

rsc.li/dalton

X-ray absorption near edge structure (XANES) spectra of blue copper proteins, amicyanin and azurin, in the solution state were measured in the copper L_3-edge energy region. The absorption peak energies were quite similar for both proteins, while the main edge region for azurin was broader than that for amicyanin, owing to more pronounced shoulder spectral features in the former. *Ab initio* calculations at the whole protein level qualitatively reproduced the experimental spectra well. The relative X-ray absorption intensities suggest that the degree of covalency of the copper–ligand bond at the active site was weaker for amicyanin than that for azurin.

Introduction

Copper is one of the transition metals widely used in many proteins and enzymes.[1] Blue copper proteins (BCPs), also known as type I copper proteins, contain single copper atoms in the active sites. The copper atom in BCPs is ligated by a sulfur atom of a cysteine residue and nitrogen atoms of two histidine residues in a trigonal planar structure and one or two weaker axial ligands, such as a sulfur atom of a methionine residue and an oxygen atom of the carbonyl group.[2] The copper atoms of amicyanin and azurin are ligated by four (H53, C92, H95, and M98) and five (G45, H46, C112, H117, and M121) residues, respectively (Fig. 1(a) and (b)). The reduction potentials of BCPs vary widely from +184 to +680 mV relative to the standard hydrogen electrode at pH 7,[3,4] despite the similarity in active site geometries. While the reduction potentials of amicyanin and azurin were reported to be around +294 and +265 mV, respectively,[5,6] it has been demonstrated that these potentials could be tuned by artificial mutations of the ligands and copper atom replacement.[6–11] For example, a five-point mutant of azurin showed the highest reduction potential (+970 mV),[10] to the best of our knowledge. Such changes in the reduction potentials are considered to arise from various contributions, including the axial copper–ligand bond length,[6,9,12] hydrogen bonding networks and hydrophobicity around the copper atom,[10,13] and solvation effects,[10] but key factors determining the reduction potentials have not yet been identified.

The structural differences among BCPs and those mutants also affect electronic structures. Previous Cu K-edge X-ray

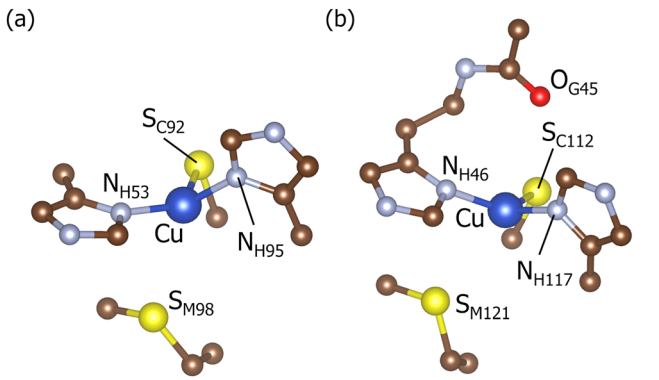

Fig. 1 Active site structures around the copper centers (blue) of amicyanin (a) and azurin (b). Labels, such as N_{H53}, indicate the corresponding ligand donor atoms for active site amino acid residues. Nitrogen (gray), sulfur (yellow), oxygen (red), and carbon (brown) atoms are shown while hydrogen atoms are omitted. Structures were visualized using VESTA.[14]

[a]*Institute for Quantum Life Science, National Institutes for Quantum Science and Technology (QST), 4-9-1 Anagawa, Inage-ku, Chiba 263-8555, Japan. E-mail: fujii.kentaro@qst.go.jp*
[b]*NanoTerasu Center, National Institutes for Quantum Science and Technology (QST), 6-6-11-901 Aoba, Aoba-ku, Miyagi 980-8579, Japan*
[c]*J-PARC Center, Japan Atomic Energy Agency, 2-4 Shirakata, Tokai, Ibaraki 319-1195, Japan*
[d]*Synchrotron Radiation Laboratory, The Institute for Solid State Physics, The University of Tokyo, 468-1 Aoba, Aoba-ku, Miyagi 980-8572, Japan*
†Electronic supplementary information (ESI) available. See DOI: https://doi.org/10.1039/d4dt02891k
‡Present affiliation: UVSOR Synchrotron Facility, Institute for Molecular Science (IMS), 38 Myodaiji, Okazaki, Aichi 444-8585, Japan
§These authors contributed equally to this work.
¶Present affiliation: Division of Electronic Structure, Department of Materials Molecular Science, Institute for Molecular Science (IMS), 38 Myodaiji, Okazaki, Aichi 444–8585, Japan

absorption near edge structure (XANES) spectroscopy demonstrated differences in the electronic structure at the copper centers of wild-type and mutant BCPs such as azurin and stellacyanin.[7,8,15] However, a comprehensive comparative survey of the electronic structure among BCPs is yet to be undertaken. The role of electronic structural changes in modulating redox activity and electron transfer is also unclear. In this work, we report the difference in the electronic structures of amicyanin and azurin wild types in the solution state using Cu L_3-edge XANES spectroscopy. The larger transition probability to 3d orbitals[16,17] at the Cu L_3-edge, compared to the K-edge, enables observation of the electronic states at the copper site in much finer detail. Theoretical XANES spectra considering whole proteins are also shown.

Experiment

Protein expression and purification

Amicyanin and azurin samples were prepared as recombinant proteins expressed in *E. coli* using the pET24a vector. Amino acid sequences coded in the vector are shown in footnote‖. DNAs were chemically synthesized and purchased from GENEWIZ (Azenta Life Sciences), optimized for *E. coli*. pET24a including the coding region was transfected into *E. coli* BL21 (DE3). The bacterial cells were grown at 310 K in LB medium containing 15 mg L^{-1} kanamycin to an OD600 of around 0.7, and protein expression was induced at 310 K for 2 hours or at 293 K for 24 hours by adding 0.1 mM isopropyl-β-D-thiogalactopyranoside for amicyanin and azurin, respectively. Furthermore, $CuSO_4$ was gradually added to the LB medium to obtain a final concentration ranging from 0.5 to 1.0 mM after the induction. The folded and soluble proteins were extracted using 20 mM Tris-HCl buffer (pH 8.0) containing 2.0 mM $CuSO_4$. The samples were purified using Ni-Sepharose gel (HisTrap FF crude CV 5 mL; Cytiva) and ion exchange columns (HiTrap Q XL and HiTrap SP XL for amicyanin and azurin, respectively; Cytiva). The protein solutions (3 mM) obtained after dialysis in 20 mM Tris-HCl buffer (pH 8.0) were used for XANES measurements.

Cu L_3-edge XANES spectroscopy

Cu L_3-edge XANES spectroscopy measurements of amicyanin and azurin in the solution state were performed using the soft X-ray spectroscopy endstation of SPring-8 BL07LSU.[18] A liquid flow cell, separated from the beamline under ultrahigh vacuum by an X-ray transmission Si_3N_4 window (150 nm thickness, 0.3 × 3 mm^2; NTT-AT, Japan), was used.[19,20] XANES spectra were acquired in total fluorescence yield mode using a silicon photodiode (SXUV100, Opto Diode, USA) at a 0.1 eV incident X-ray energy resolution.

Theoretical calculations

The crystal structures of amicyanin and azurin were obtained from the Protein Data Bank (ID: 2OV0 and 4AZU, respectively).[11,21] Missing hydrogen atoms were supplemented in the crystal structures using a semiempirical quantum chemistry program MOPAC2016.[22] Each single protein molecule was considered for the following calculations. Geometry optimization for the whole protein molecule was done based on the MOZYME method,[23,24] as implemented in the MOPAC program, using the semiempirical Hamiltonian PM7.[24] The solvent effect of water was incorporated using the conductor-like screening model (COSMO). During the optimization, the position of copper atoms was fixed.

XANES spectra were calculated for the whole proteins (1607 and 1933 atoms for amicyanin and azurin, respectively) in the Cu L_3-edge energy region based on multiple scattering theory assuming a muffin-tin potential using an *ab initio* calculation code FDMNES.[25] The electronic structures were calculated inside spheres centered on the copper atom with 30.0 and 35.0 Å radii for amicyanin and azurin, respectively. The spheres included the whole proteins for both cases. To account for the solvent effect, the maximum potential was restricted ($V_{max} = -6$). Spectral convolution was applied to the region 3 eV above the Fermi level (E_F) to reproduce the experimental spectra well. For other parameters, default values were used. The partial density of states (pDOS) profiles derived from the Cu and ligand donor atoms were also calculated. For comparisons, XANES spectra of amicyanin and azurin using the coordinates in crystal structures and those optimized without the solvent effect were also calculated based on the same procedure.

Results and discussion

Experimental and theoretical Cu L_3-edge XANES spectra

Fig. 2(a) and (b) show the conformations of amicyanin and azurin, respectively, before (crystal structure)[11,21] and after the geometry optimization considering the solvent effect (solution structure). Structural changes throughout the protein owing to the geometrical optimization considering the solvent effect were anticipated though the water molecules existed around the proteins in the crystals. Distances between the copper and each ligand atom also changed by *ca.* 0.1–0.5 Å. Comparisons with the structures optimized without the solvent effect are shown in the ESI.† Fig. 3(a) and (b) show the theoretical Cu L_3-edge XANES spectra of amicyanin and azurin, respectively, in their crystal and solution structures. The difference in spectral profiles primarily originates from structural changes in the

‖Amino acid sequences coded in the vector for this study. The underlines indicate tag sequence for production in *E. coli* and purification.

Amicyanin (141aa):
MKWSHPQFEKHHHHHHKTDKTDKTDKTDKTDDDDKGDKATIPSESPFAAAEVADGAIVVDIAKMKYETPELHVKVGDTVTWINREAMPHNVHFVAGVLGEAALKGPMMKKEQAYSLTFTEAGTYDYHCTPHPFMRGKVVVE

Azurin (176aa):
MAKKTSSKGKWSHPQFEKHHHHHHKTDKTDKTDKTDKTDDDDKSSSGGAECSVDIQGNDQMQFNTNAITVDKSCKQFTVNLSHPGNLPKNVMGHNWVLSTAADMQGVVTDGMASGLDKDYLKPDDSRVIAHTKLIGSGEKDSVTFDVSKLKEGEQYMFFCTFPGHSALMKGTLTLK

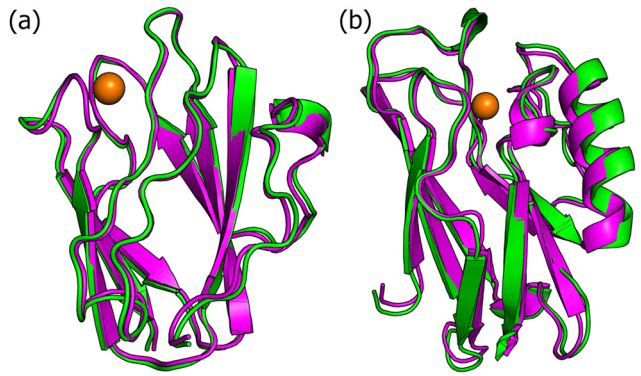

Fig. 2 The crystal (green) and solution structures (magenta) of amicyanin (a) and azurin (b). Copper atoms are shown in orange. PyMOL software (https://www.pymol.org/) was used.

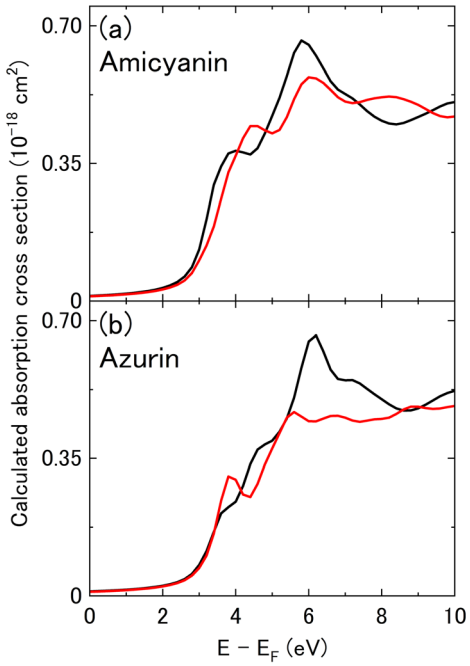

Fig. 3 Theoretical Cu L_3-edge XANES spectra of amicyanin (a) and azurin (b) in crystal (red) and solution (black) structures.

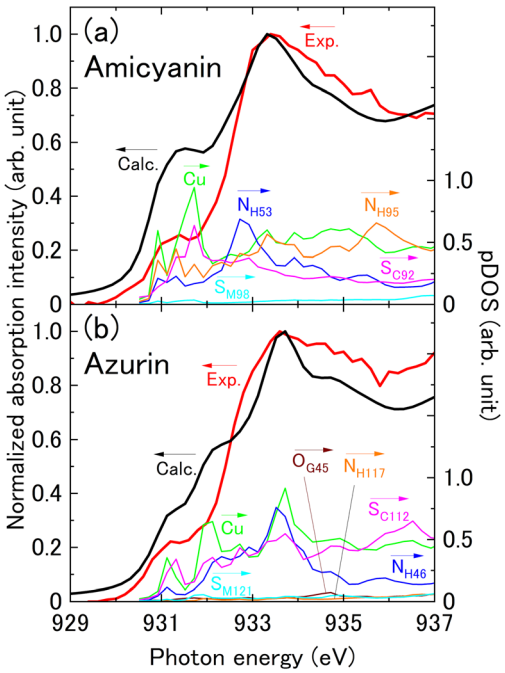

Fig. 4 Experimental (red) and theoretical (black) Cu L_3-edge XANES spectra (left axis) of amicyanin (a) and azurin (b) in the solution state. The pDOS spectra (right axis) are also shown: Cu (green), N_{H53} and N_{H46} (blue), S_{C92} and S_{C112} (magenta), N_{H95} and N_{H117} (orange), S_{M98} and S_{M121} (cyan), and O_{G45} (brown).

protein, particularly those involving bond distances between the Cu and each ligand donor atom. The calculated XANES spectra for solution structures reproduced experimental spectral profiles better than those calculated for crystal structures as shown hereafter. It implies that the geometry optimization, including the solvent effect, is an important procedure for XANES calculations in the solution state.

Fig. 4(a) and (b) show the experimental and theoretical Cu L_3-edge XANES spectra of amicyanin and azurin, respectively. The theoretical spectra were based on the solution structures as mentioned above. The pDOS values for each ligand donor atom of amicyanin and azurin are also shown. The absorption energies of theoretical XANES spectra were shifted to fit the largest absorption peaks of the experimental spectra. Amicyanin exhibited two peaks at 931.2 and 933.4 eV (Fig. 4(a)). A shoulder structure was also observed at around 935 eV. The theoretical calculation qualitatively reproduced the experimental spectrum well. The differences in the absorption intensities would be caused by the difference in experimental and theoretical conditions, such as amicyanin in Tris-HCl buffer *vs.* in the hypothetical solvent. Focusing on the pDOS intensities of ligand atoms, S_{C92} and N_{H95} dominate at around 931–932 eV (Fig. 4(a)). The first peak at 931.2 eV mainly originated from the transitions from the Cu $2p_{3/2}$ orbital to antibonding states involving hybridized orbitals of Cu–S_{C92} and Cu–N_{H95}. In turn, the second peak at 933.4 eV was assigned to the transition from the Cu $2p_{3/2}$ orbital to antibonding states involving Cu–N_{H53} and Cu–N_{H95} hybridized orbitals. The Cu $2p_{3/2}$ transition to the antibonding state of Cu–N_{H95} mainly contributed to the shoulder structure at around 935 eV. It is noted that the pDOS contribution from S_{M98} was lower in the measurement region, suggesting the minimal XANES contribution from the axial ligand.

For azurin, the experimental spectrum exhibited two peaks at 931.2 and 933.6 eV and shoulder structures around 932.8 and 935 eV (Fig. 4(b)). Although the peak corresponding to the experimental shoulder structure at 932.8 eV was predicted at a lower energy (~932 eV), the theoretical calculation for azurin also reproduced the experimental spectrum qualitatively. The pre-edge peak at 931.2 eV and the second shoulder structure at 935 eV mainly arise from the transition from Cu $2p_{3/2}$ to an

antibonding state derived from hybridized orbitals involving Cu and S_{C112}. In turn, the main peak at 933.6 eV was mainly assigned to the transition from Cu $2p_{3/2}$ to the antibonding orbitals involving Cu and N_{H46}. The first shoulder structure at 932.8 eV originated from the transitions to antibonding states involving Cu–N_{H46} and Cu–S_{C112}. Similar to amicyanin, the axial ligands only have a small contribution to the XANES spectra because the corresponding pDOS values due to O_{G45} and S_{M121} were also quite small. Of note is the difference in the relative pDOS contributions of the nitrogen ligands for amicyanin and azurin. In amicyanin, the pDOS values due to N_{H53} and N_{H95} were both equally strong, particularly when compared to the axial ligand contribution (S_{M98}). In contrast, for azurin, the pDOS contribution due to N_{H46} was greater compared to the other histidine nitrogen N_{H117}, with the latter being almost comparable to the nearly negligible pDOS contributions from the axial ligand donors S_{M121} and O_{G45}. Thus, the theoretical calculations predicted that the DOS of amicyanin spread throughout the trigonal planar structure composed of two nitrogen and one sulfur ligands (N_{H53}, N_{H95}, and S_{C92}), while that of azurin was relatively localized around two out of three trigonal ligand atoms (N_{H46} and S_{C112}). The extra axial ligand of azurin (O_{G45}) may affect the difference in the DOS distributions. The reduction potentials of BCPs vary despite the similarity of the copper ligand structure as mentioned above. These may originate from the differences in such DOS distributions. More precise theoretical work is required to discuss these differences and their origins. Understanding the properties of BCPs including their reduction potentials is an important direction for future research.

Metal–ligand bond covalency at the active site

The Cu L_3-edge XANES intensity, for the most part, is determined by the degree to which the Cu $2p_{3/2} \rightarrow 3d$ transition is electric dipole-allowed.[26] Particularly around the pre-edge at *ca*. 931.2 eV, the Cu L_3-edge XANES intensity mainly derives from the d character of the lowest unoccupied molecular orbital (LUMO) accessed under X-ray excitation. It reflects the extent of overlap between the Cu 3d orbitals and the interacting ligand orbitals of mostly p character.[16,17] For a model copper complex, such as the active sites of amicyanin and azurin, the ansatz wave function for the LUMO responsible for the Cu L_3-edge XANES pre-edge peak can be adopted as

$$\varphi_{\mathrm{LUMO}} = \sqrt{1-\beta^2}\varphi_{\mathrm{Cu_{3d}}} - \beta\varphi_{\mathrm{ligand_{np}}},$$

where β^2 is a measure of the metal–ligand bond covalency, that is, the extent of covalent interaction and orbital hybridization between the metal and the ligand orbitals $\varphi_{\mathrm{Cu_{3d}}}$ and $\varphi_{\mathrm{ligand_{np}}}$, respectively. The minus sign indicates that the metal–ligand orbital interaction in the LUMO is antibonding.[16,17] As the strength of the metal–ligand covalent interaction (β^2) becomes larger, the ligand orbital $\varphi_{\mathrm{ligand_{np}}}$ contribution to the LUMO also becomes greater. Consequently, the metal orbital $\varphi_{\mathrm{Cu_{3d}}}$ contribution to the LUMO, given by $(1 - \beta^2)$, becomes smaller, and the Cu 3d orbital population that can participate in the absorption transition also decreases. Hence, this leads to a decrease in the corresponding XANES intensity.

We adopt here an analysis of metal–ligand bond covalency at the copper active sites from the observed XANES pre-edge intensities.[16,17] Amicyanin exhibited a slightly higher pre-edge intensity compared to azurin (Fig. S4†). The XANES pre-edge intensity ratio, $I_{\mathrm{am}}/I_{\mathrm{az}}$, for amicyanin ($I_{\mathrm{am}}$) and azurin ($I_{\mathrm{az}}$) was *ca.* 1.1 at 931.2 eV. The pre-edge intensity ratio is correlated with the covalency values as

$$\frac{I_{\mathrm{am}}}{I_{\mathrm{az}}} = \frac{1-{\beta_{\mathrm{am}}}^2}{1-{\beta_{\mathrm{az}}}^2}$$

It implies that the metal–ligand bond covalency in amicyanin is lower than that in azurin ($\beta_{\mathrm{am}} < \beta_{\mathrm{az}}$). This suggests that the metal–ligand bonds of amicyanin were weaker than those of azurin; that is, the electrons in the amicyanin active site appear to be relatively localized in the Cu center, while the electrons in the azurin active site appear to be relatively delocalized into the ligand orbitals. Calculations (Fig. 4(a) and (b)) also showed that from the integrated area of the pDOS under the pre-edge energy region of which the ligand-to-Cu ratio was 0.59 and 0.64 for amicyanin and azurin, respectively. This further supports that, compared to azurin, the amicyanin copper active sites have a weaker metal–ligand bond with less covalency and the electrons are fairly localized at the Cu center.

The behavior of main-edge spectral intensities, primarily derived from ligand orbitals, further corroborates the above observation. With the greater Cu–ligand bond covalency in azurin ($\beta_{\mathrm{am}} < \beta_{\mathrm{az}}$) and the accompanying electron delocalization into the ligand orbitals, compared to amicyanin, azurin exhibited stronger main-edge intensities, as reflected in the more pronounced shoulder-like features in the experimental XANES spectra at around 935 eV (Fig. S4†). These results again confirm that the metal–ligand bond in amicyanin is weaker and less covalent than that in azurin, albeit from the viewpoint of the ligand, instead of the Cu d orbitals. Furthermore, the above analysis remains consistent with previous computational work[27] on azurin mutants, suggesting that a decrease in covalency resulted in an increase in reduction potential, given that amicyanin (+294 mV) is observed to have a higher reduction potential than azurin (+265 mV).[5,6] It is noted that the calculated XANES spectra for the crystal and solution structures exhibit different metal–ligand bond covalency behavior, suggesting that the electronic properties of copper proteins in the biologically relevant solution state could be different from those in the solid state observed in crystal structures. We remark that the liquid flow cell XANES measurements on protein solutions implemented in this work provide a precedent for future directions of biological relevance, including drug development,[28,29] time-resolved spectroscopy,[30,31] and single-cell profiling.[32]

Conclusions

The observed differences in experimental Cu L_3-edge XANES intensities for amicyanin and azurin blue copper proteins are

consistent with the density of states and Cu–ligand bond covalency predicted from *ab initio* electronic structure calculations performed at the whole protein level. Furthermore, it is noted that this work is the first experimental observation of the XANES spectra of copper proteins in the solution state in the Cu L_3-edge soft X-ray regime. Lastly, the possible role of metal–ligand bond covalency in the observed difference in reduction potential between amicyanin and azurin was elaborated.

Author contributions

Y. I.: formal analysis, investigation, visualization, and writing – original draft; R. U.: investigation and writing – original draft; J. M.: investigation and writing – original draft; C. S.: resources; M. A.: resources and writing – original draft; N. K.: investigation and writing – original draft; H. K. investigation and writing – original draft; Y. H.: investigation and writing – original draft; K. F.: conceptualization, funding acquisition, project administration, investigation, and writing – original draft.

Data availability

The data supporting this article have been included as part of the ESI.†

Conflicts of interest

There are no conflicts to declare.

Acknowledgements

XANES spectroscopy was performed using the SPring-8 BL07LSU of the Institute for Solid State Physics, the University of Tokyo (No. 2021B7438). This work was also carried out in part through SPring-8 proposals 2018B3852 and 2019A3852. This work was financially supported by the MEXT Quantum Leap Flagship Program (MEXT Q-LEAP) Grant Number JPMXS0120330644 and the QST-Tohoku University Matching Research Support Project. This work was partially supported by the J-PARC MLF Deuteration Laboratory and Ms Rumi Shimizu at QST for the preparation of protein samples.

References

1 E. I. Solomon, D. E. Heppner, E. M. Johnston, J. W. Ginsbach, J. Cirena, M. Qayyum, M. T. Kieber-Emmons, C. H. Kjaergaard, R. G. Hadt and L. Tian, *Chem. Rev.*, 2014, **114**, 3659.
2 H. B. Gray, B. G. Malmström and R. J. P. Williams, *J. Biol. Inorg. Chem.*, 2000, **5**, 551.
3 N. Sailasuta, F. C. Anson and H. B. Gray, *J. Am. Chem. Soc.*, 1979, **101**, 455.
4 W. J. Ingledew and J. G. Cobley, *Biochim. Biophys. Acta*, 1980, **590**, 141.
5 K. A. Gray, D. B. Knaff, M. Husain and V. L. Davidson, *FEBS*, 1986, **207**, 239.
6 N. M. Marshall, D. K. Garner, T. D. Wilson, Y.-G. Gao, H. Robinson, M. J. Nilges and Y. Lu, *Nature*, 2009, **465**, 113.
7 L. M. Murphy, R. W. Strange, B. G. Karlsson, L. G. Lundberg, T. Pascher, B. Reinhammar and S. S. Hasnain, *Biochemistry*, 1993, **32**, 1965.
8 S. DeBeer, C. N. Kiser, G. A. Mines, J. H. Richards, H. B. Gray, E. I. Solomon, B. Hedman and K. O. Hodgson, *Inorg. Chem.*, 1999, **38**, 433.
9 J. K. Ma, F. S. Mathews and V. L. Davidson, *Biochemistry*, 2007, **48**, 8561.
10 P. Hosseinzadeh, N. M. Marshall, K. N. Chacón, Y. Yu, M. J. Nilges, S. Y. New, S. A. Tashkov, N. J. Blackburn and Y. Lu, *Proc. Natl. Acad. Sci. U. S. A.*, 2016, **113**, 262.
11 S.-J. Jo, S. Shin and M. Choi, *Appl. Biol. Chem.*, 2018, **61**, 181.
12 M. Choi, N. Sukumar, A. Liu and V. L. Davidson, *Biochemistry*, 2009, **48**, 9184.
13 A. Donaire, B. Jiménez, C. O. Femández, R. Pierattelli, T. Niizeki, J.-M. Moratal, J. F. Hall, T. Kohzuma, S. S. Hasnain and A. J. Vila, *J. Am. Chem. Soc.*, 2002, **124**, 13698.
14 K. Momma and F. Izumi, *J. Appl. Crystallogr.*, 2011, **44**, 1272.
15 S. DeBeer George, L. Basumallick, R. K. Szilagyi, D. W. Randall, M. G. Hill, A. M. Nersissian, J. S. Valentine, B. Hedman, K. O. Hodgson and E. I. Solomon, *J. Am. Chem. Soc.*, 2003, **125**, 11314.
16 S. DeBeer George, M. Metz, R. K. Szilagyi, H. Wang, S. P. Cramer, Y. Lu, W. B. Tolman, B. Hedman, K. O. Hodgson and E. I. Solomon, *J. Am. Chem. Soc.*, 2001, **123**, 5757.
17 M. F. Qayyum, R. Sarangi, K. Fujisawa, T. D. P. Stack, K. D. Karlin, K. O. Hodgson, B. Hedman and E. I. Solomon, *J. Am. Chem. Soc.*, 2013, **135**, 17417.
18 Y. Harada, M. Kobayashi, H. Niwa, Y. Senba, H. Ohashi, T. Tokushima, Y. Horikawa and S. Shin, *Rev. Sci. Instrum.*, 2012, **83**, 013116.
19 Y. Harada, J. Miyawaki, H. Niwa, K. Yamazoe, L. G. M. Pettersson and A. Nilsson, *J. Phys. Chem. Lett.*, 2017, **8**, 5487.
20 R. Ugalino, K. Yamazoe, J. Miyawaki, H. Kiushi, N. Kurahashi, Y. Kosegawa and Y. Harada, *J. Synchrotron Radiat.*, 2024, **31**, 217.
21 H. Nar, A. Messerschmidt, R. Huber, M. van de Kamp and G. W. Canters, *J. Mol. Biol.*, 1991, **221**, 765.
22 James J. P. Stewart, MOPAC2016, Stewart Computational Chemistry, Colorado Springs, CO, USA, 2016, **https://openmopac.net/**.
23 J. J. P. Stewart, *Int. J. Quantum Chem.*, 1996, **58**, 121.
24 J. J. P. Stewart, *J. Mol. Model*, 2013, **19**, 1.
25 O. Bunău and Y. Joly, *J. Phys.: Condens. Matter*, 2009, **21**, 345501.

26 P. A. M. Dirac, *Proc. R. Soc. A*, 1927, **114**, 243.
27 R. G. Hadt, N. Sun, N. M. Marshall, K. O. Hodgson, B. Hedman, Y. Lu and E. I. Solomon, *J. Am. Chem. Soc.*, 2012, **134**, 16701.
28 Y. Izumi, M. Ohara, K. Fujii, A. Yokoya and M. Ogawa, *Chem. Phys. Lett.*, 2023, **822**, 140508.
29 M. Ohara, Y. Izumi, H. Takakura, S. Enomoto, K. Fujii, A. Yokoya and M. Ogawa, *Radiat. Phys. Chem.*, 2024, **216**, 111394.
30 Z. Yin, Y. Chang, T. Balciunas, Y. Shakya, A. Djorovic, G. Gaulier, G. Fazio, R. Santra, L. Inhester, J. Wolf and H. Worner, *Nature*, 2023, **619**, 749.
31 A. Mondal, O. Neufeld, Z. Yin, Z. Nourbakhsh, V. Svoboda, A. Rubio, N. Dejean and H. Worner, *Nat. Phys.*, 2023, **19**, 1813.
32 T. Shimada, K. Fujino, T. Yasui, N. Kaji, Y. Ueda, K. Fujii, H. Yukawa and Y. Baba, *Anal. Chem.*, 2023, **95**, 18335.